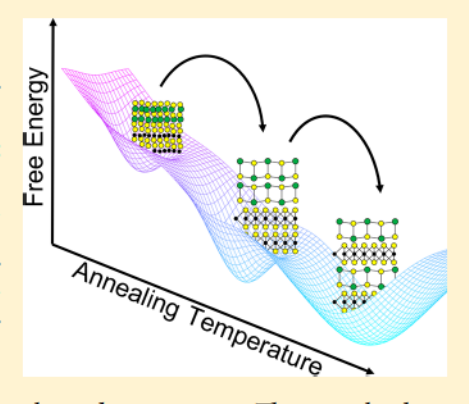


Kinetically Controlled Formation and Decomposition of Metastable $[(BiSe)_{1+\delta}]_m[TiSe_2]_m$ Compounds

Alexander C. Lygo, Danielle M. Hamann, Daniel B. Moore, Devin R. Merrill, Jeffrey Ditto, Marco Esters, ^{†©} Jacob Orlowicz, [†] Suzannah R. Wood, ^{†,§©} and David C. Johnson*, ^{†©}

Department of Chemistry, Materials Science Institute, University of Oregon, Eugene, Oregon 97403, United States §XTD-IDA, Los Alamos National Lab, Los Alamos, New Mexico 87545, United States

ABSTRACT: Preparing homologous series of compounds allows chemists to rapidly discover new compounds with predictable structure and properties. Synthesizing compounds within such a series involves navigating a free energy landscape defined by the interactions within and between constituent atoms. Historically, synthesis approaches are typically limited to forming only the most thermodynamically stable compound under the reaction conditions. Presented here is the synthesis, via self-assembly of designed precursors, of isocompositional incommensurate layered compounds $[(BiSe)_{1+\delta}]_m[TiSe_2]_m$ with m = 1, 2, and 3. The structure of the BiSe bilayer in the m = 1 compound is not that of the binary compound, and this is the first example of compounds where a BiSe layer thicker than a bilayer in heterostructures has been prepared. Specular and in-plane X-ray diffraction combined with high-resolution electron microscopy data was used to follow the formation of the compounds during low-temperature annealing and the



subsequent decomposition of the m = 2 and 3 compounds into $[(BiSe)_{1+\delta}]_1[TiSe_2]_1$ at elevated temperatures. These results show that the structure of the precursor can be used to control reaction kinetics, enabling the synthesis of kinetically stable compounds that are not accessible via traditional techniques. The data collected as a function of temperature and time enabled us to schematically construct the topology of the free energy landscape about the local free energy minima for each of the products.

INTRODUCTION

Homologous series of compounds, compounds related by a common structural module that expands in regular increments, are common in both organic and inorganic chemistry. These series enable chemists to extrapolate chemical information to predict potential structures of compounds that have yet to be prepared. This is particularly important in inorganic chemistry, where examples of homologous series include both simple oxides $(M_nO_{2n-1}, \text{ where } M = \text{Ti, V; } Mo_nO_{3n-1}, W_nO_{3n-2}),$ complex oxides (the Ruddlesden-Popper homologous series, including $Sr_{n+1}M_nO_{3n+1}$, where M=Co, Ti, Ru, and Mn), and chalcogenide systems. ¹⁻⁵ The common structural modules that define inorganic homologous series are typically fragments of known structures, such as the rock salt structure. Different structural modules can be obtained from the same bulk structure simply by altering the direction of fragmentation (such as along 100 or 111 in a rock salt structure). The different building blocks typically lower the total free energy by distorting to create commensurate interfaces. Using chemically stable structural fragments as building blocks to predict structures of novel compounds can be a powerful tool, as illustrated by the work of Cario and co-workers. They used the criteria of commensurate interfaces between two-dimensional building blocks and charge balance to target and discover new inorganic compounds. However, this approach is not limited to compounds with commensurate interfaces, as compounds with incommensurate interfaces can form if the interaction between

layers is large enough to create a local free energy minimum. Perhaps the most studied of these are the misfit layer compounds, which consist of dichalcogenide layers alternating with rock salt structured layers. Inter- and intralayer interactions cause these compounds to form one commensurate and one incommensurate axis.

The interactions both within and between building blocks define the energy landscape, which contains both global and local free energy minima corresponding to thermodynamically and kinetically stable compounds, respectively.^{8,9} At commensurate interfaces, the interactions between layers are defined by the systematic coordination of interfacial atoms by both structural fragments. For a commensurate interface to form, the distorted compound must be lower in free energy than the undistorted analogue. At incommensurate interfaces, understanding the interaction between layers is more challenging and has been discussed extensively in the misfit layer compound literature. The consensus is that charge transfer between the layers results in an ionic "capacitive" interaction between the constituents that stabilizes the structure, although entropic stabilization from cation disorder has also been proposed.¹⁰⁻¹⁵ For an incommensurate interface to form, the interaction between the layers must be large enough to stabilize the compound in spite of the irregular bond distances and angles

Received: December 21, 2017 Published: February 12, 2018

between atoms at the interface. Utilizing building blocks that readily form incommensurate interfaces significantly expands the number of homologous series that can be imagined.

While homologous series provide the ability to predict potential compounds and their structure, it is often not possible to prepare them via traditional high-temperature synthesis methods, which is especially frustrating if one or more members of a potentially homologous series of compounds are known. This is particularly true when the homologous series of compounds have the same overall stoichiometry. A synthetic challenge is to understand how to assemble building blocks and order them into the targeted arrangement. Several lowtemperature synthesis approaches have successfully been used to prepare compounds not accessible via high-temperature solid-state or vapor transport reactions. The most common approach has been using fluxes to reduce reaction temperatures while simultaneously empirically adjusting the composition of the melt, the annealing temperature, and annealing time to prepare targeted homologues.⁵ Another approach is to first "prefabricate" structural modules and then find conditions that result in their self-assembly in a desired spatial arrangement. 16 A third method for targeting homologous series is to prepare a designed precursor with compositional periodicity mimicking the desired building blocks and then determine the conditions that allow the compound to self-assemble into the desired product.¹⁷ Additionally, traditional and van der Waals epitaxy have been used to successfully prepare series of compounds. 18 All of these approaches would benefit from a greater understanding of the reaction mechanisms and the energy landscape around targeted compounds.

Here we study the reaction pathway of precursors designed to form $[(BiSe)_{1+\delta}]_m[TiSe_2]_m$ compounds where m = 1, 2, and 3. $[(BiSe)_{1+\delta}]_1[TiSe_2]_1$ is thermodynamically stable relative to a mix of binary compounds and has been prepared using traditional high-temperature solid-state and vapor transport reactions. $[(BiSe)_{1+\delta}]_1[TiSe_2]_1$ prepared at high temperature is a misfit layer compound with one incommensurate axis. Its stability is a consequence of charge transfer from the BiSe layer (containing nominally Bi3+ cations) to the TiSe2 layer. 19-21 $[(BiSe)_{1+\delta}]_1[TiSe_2]_1$ has also been prepared from designed precursors, resulting in a rotationally disordered layer compound with two incommensurate axes.2 $[Se)_{1+\delta}]_m[TiSe_2]_m$ where m=2 and 3 have not been previously reported, and to our knowledge there have been no reports of misfit layer compounds with $m \ge 1$ when the rock salt constituent contains Bi or a trivalent cation such as a lanthanide. Specular X-ray diffraction and in-plane X-ray diffraction data, collected as a function of annealing temperature, revealed the evolution of the superstructure and the structure of the constituents, respectively. High-resolution electron microscopy images, collected pre- and postdecomposition, resolved the local structure of the m = 2 compound. All three compounds begin to self-assemble at low temperatures, with $[(BiSe)_{1+\delta}]_2[TiSe_2]_2$ and $[(BiSe)_{1+\delta}]_3[TiSe_2]_3$ decomposing into $[(BiSe)_{1+\delta}]_1[TiSe_2]_1$. $[(BiSe)_{1+\delta}]_m[TiSe_2]_m$ becomes increasingly unstable with respect to transforming into $[(BiSe)_{1+\delta}]_1[TiSe_2]_1$ as m is increased. These data were used to construct a schematic free energy landscape containing each of the targeted compounds.

EXPERIMENTAL SECTION

Amorphous precursors were synthesized simultaneously on silicon substrates and poly(methyl methacrylate) (PMMA)-coated Si wafers, using a custom-built physical vapor deposition system. Elemental Bi and Ti were deposited using electron beam guns, and Se was deposited using a Knudsen effusion cell. Pressure was maintained below 5×10^{-7} Torr during deposition. The deposition rates of each source and the thickness of the elemental layers were independently measured using quartz crystal microbalances. Computer-controlled pneumatic shutters placed above each source regulated the elemental layer thickness and sequence. Layers of each element were deposited on the substrate in the order of $(Ti-Se)_m$ - $(Bi-Se)_m$ where m=1, 2, and 3, and each sequence was repeated to obtain a total film thickness of approximately 50 nm. The composition and thicknesses of the Ti-Se and Bi-Se were calibrated as described in detail by Atkins et al. as well as briefly below.²³ Samples on the silicon were annealed at specified temperatures for 30 min in a nitrogen atmosphere with oxygen below 1.0 ppm. Electron-probe microanalysis (EPMA) was used to determine the composition of the thin film samples on silicon.²

Freestanding films for calorimetry measurements were prepared from the films deposited on the PMMA-coated substrates by dissolving the PMMA using acetone and filtering out the film particles using a Teflon filter. Differential scanning calorimetry (DSC) data were collected on a Netzsch STA 409 PC Luxx thermal analyzer using 1-3 mg of freestanding film, which was placed into an aluminum pan and sealed by crimping. Samples were heated from ambient temperatures to 400 °C at rates of 15 °C/min under a flow of nitrogen and then cooled back to room temperature. Without disturbing the sample or instrument, this cycle was repeated to measure reversible transitions in the sample as well as the cell background. The net heat flow, associated with the irreversible changes occurring in the sample during the initial heating cycle, was determined by subtracting the data collected during the second cycle from those for the first. To check for reproducibility in the cell background, a third cycle was collected and compared to the second

X-ray reflectivity (XRR) and specular X-ray diffraction (XRD) patterns were measured on a Bruker D8 Discover diffractometer with Cu K α radiation, equipped with a Göbel mirror. Grazing incidence inplane X-ray diffraction patterns were acquired on a Rigaku Smartlab (Cu Kα) diffractometer and on the Multi-Purpose General Scattering beamline 33-BM-C (λ = 1.2653 Å) at the Advanced Photon Source at Argonne National Laboratory. X-ray fluorescence measurements were performed on a Rigaku ZSX Primus-II with a rhodium X-ray source. For the m = 1 compound the c-axis lattice parameters were calculated using modified Braggs' law. Least-squares fits of the in-plane lattice parameters (a and b) of TiSe₂ and BiSe were done using the WinCSD software package. 25 In-plane lattice parameters (a and b) of TiSe2 and BiSe and the c-axis lattice parameters were refined using full pattern Le Bail fits done in the FullProf Suite. $^{26-28}$

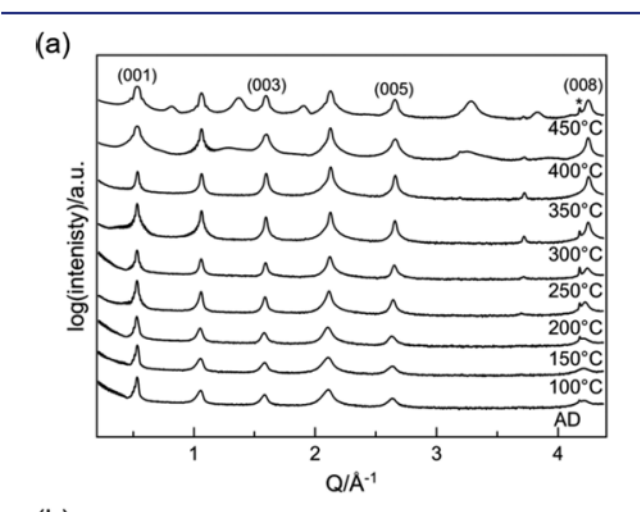
Scanning transmission electron microscopy (STEM) cross sections were prepared on an FEI Helios 600-dual beam focused ion beam (FIB) with a side winder ion column using backside milling methods² and wedge premilling methods. 30 High-angle annular dark field STEM (HAADF-STEM) was performed on an FEI Titan 80-300 TEM/ STEM at 300 keV.

RESULTS AND DISCUSSION

Layered precursors were prepared with compositional modulation that mimics the target compounds, $[(BiSe)_{1+\delta}]_m[TiSe_2]_m$ m = 1, 2, and 3. A calibration procedure was used to determine the deposition parameters (local compositions, layer thicknesses, and layer sequences) required to crystallize the desired products.²³ Briefly, the ratio of the elements in binary Bi-Se and Ti-Se multilayer films was calibrated by keeping the amount of Se constant in each bilayer and varying the thickness of the metal. The thickness and atomic composition were determined via XRR and EPMA, respectively, and the ratio of the deposition thicknesses was chosen to match the 1:1 stoichiometry of BiSe and the 1:2 stoichiometry of TiSe2. The ratio of Bi/Ti was adjusted to match the misfit (1.15) of the

previously reported (BiSe)_{1.15}TiSe₂ compound²² by preparing samples with a Bi-Se-Ti-Se sequence that held the metal to Se ratios in each layer constant and varied the thickness of one of the constituent layers. XRR and EPMA were used to determine the deposition parameters required to obtain the desired misfit. The thicknesses of the (Bi-Se), and (Ti-Se), bilayers were adjusted to correct the absolute thickness to yield one layer of BiSe and one layer of TiSe, as determined by the quality of the diffraction pattern of $[(BiSe)_{1+\delta}]_1[TiSe_2]_1$, which self-assembled on annealing. To prepare precursors designed to form the m = 2 and 3 compounds, the layer sequences Bi–Se– Bi-Se-Ti-Se-Ti-Se and Bi-Se-Bi-Se-Bi-Se-Ti-Se-Ti-Se-Ti-Se were deposited using the deposition parameters of the m = 1 compound until films of approximately 50 nm were obtained.

To characterize the evolution of the superstructure and individual constituent structures upon heating the (BiSe)1-(TiSe₂)₁ precursor, specular (Figure 1a) and in-plane (Figure



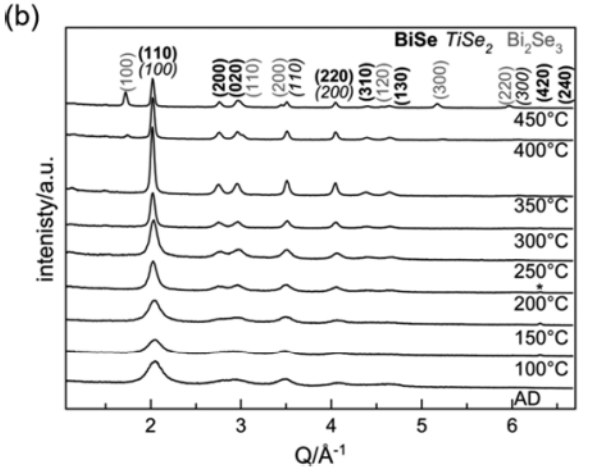


Figure 1. (a) Specular and (b) in-plane X-ray diffraction patterns for a (Ti-Se)₁-(Bi-Se)₁ precursor after annealing at each temperature for 30 min.

1b) X-ray diffraction were collected. At low annealing temperatures, the specular scan has intensity maxima from two sources. At small Q values there are sharp reflections from the periodic modulation of the electron density resulting from the sequential deposition of the elements. At larger Q values, there are broader maxima due to the crystallization of the constituents.31 The first reflection yields a c-axis lattice

parameter that is approximately 0.08 Å smaller than the c-axis lattice parameter corresponding to the higher order reflections. For annealing temperatures between 150 and 250 °C, diffusion results in growth of the targeted $[(BiSe)_{1+\delta}]_1[TiSe_2]_1$ product, and the reflections due to the artificial modulation gradually shift to positions corresponding to a single family of 00l reflections. Concurrently, the broader maxima sharpen and gain intensity, and additional reflections are resolved, indicating the BiSe and TiSe₂ layers become more coherent with one another. The c-axis lattice parameter decreases between annealing temperatures of 150 and 250 °C, consistent with atoms diffusing to form atomic planes expected for the BiSe and TiSe₂ structures. Above 250 °C the c-axis lattice parameter remains constant, within error. Lattice parameters are summarized in Table 1 and are consistent with those previously reported.²

Table 1. Lattice Parameters for the (Ti-Se)₁-(Bi-Se)₁ Precursor after Annealing for 30 min at Various Temperatures

annealing temp (°C)	c (Å)	BiSe a (Å)	BiSe b (Å)	TiSe ₂ a (Å)
AD	11.94(2)	4.52(1)	4.23(1)	3.56(2)
100	11.94(2)	4.54(2)	4.25(2)	3.56(2)
150	11.94(2)	4.521(8)	4.238(7)	3.59(1)
200	11.894(8)	4.547(4)	4.244(3)	3.587(4)
250	11.84(1)	4.533(4)	4.234(3)	3580(5)
300	11.821(4)	4.557(2)	4.242(1)	3.579(2)
350	11.81(2)	4.564(2)	4.246(1)	3.580(3)
400	11.83(2)	4.551(2)	4.244(1)	3.589(3)
450	11.822(4)	4.548(1)	4.251(1)	3.583(1)

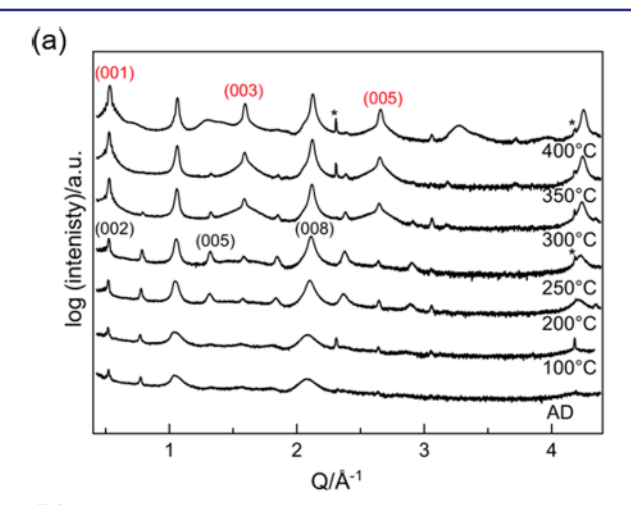
The in-plane diffraction data provide information on the structures of the constituent layers in the compound. All reflections can be indexed as hk0 reflections of either BiSe or TiSe2, with no observable Bi2Se3 reflections until after annealing at 400 °C. The scan of the as-deposited precursor contains broad reflections characteristic of small grains for both BiSe and TiSe₂. When comparing the TiSe₂ (110) and BiSe (200) reflections in the as-deposited film, a greater relative intensity and narrower line width are initially observed for the TiSes reflections, indicating that more crystalline TiSe2 forms during deposition relative to BiSe. As the annealing temperature is increased, the intensity of the in-plane reflections for both BiSe and TiSe2 increases. The splitting of the BiSe reflection, at approximately 3 Å-1, indicates that the in-plane unit cell is rectangular, and the increase in the splitting with increasing annealing temperature indicates that the difference between the a- and b-axis lattice parameters increases. The in-plane areas of both constituents increase slightly as the annealing temperature is increased.

After annealing at 450 °C, additional reflections are observed in both the specular and in-plane diffraction patterns that indicate that an impurity phase of Bi₂Se₃, which is crystallographically aligned to the substrate, forms. When comparing Xray fluorescence measurements collected after annealing at 300 and 450 °C, a ~40% decrease in Se counts and a significant increase in integrated O counts were observed, without significant changes in the Bi or Ti intensities. If all the TiSe, was converted to TiO₂ one would expect a 63.5% decrease in Se counts, assuming a misfit of 1.15. This suggests that the Bi₂Se₃ results from partial destruction of the superlattice as TiSe2 is converted to TiO2, which is consistent with the decrease in the in-plane intensity of TiSe2 reflections after annealing at 450 °C. The TiO2 is not observed in the diffraction pattern either because it is amorphous or because the grain sizes are too small to be observed relative to the other, crystallographically aligned compounds. A balanced chemical equation for this conversion is

2[(BiSe)<sub>1+
$$\delta$$</sub>]₁[TiSe₂]₁ + 2O₂
 \rightarrow (1 + δ)Bi₂Se₃ + 2TiO₂ + (3 - δ)Se

where bismuth and selenium are being oxidized. Some of the selenium that is not reacted to form Bi₂Se₃ could be further oxidized to form SeO2.

An annealing study was performed on the (Ti-Se)2-(Bi-Se)₂ precursor (Figure 2) to ascertain the conditions required



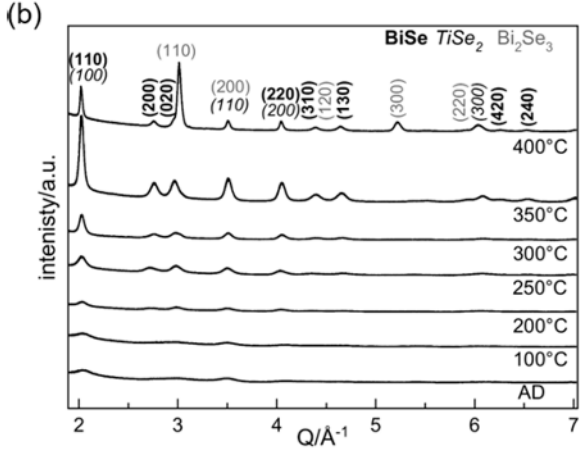


Figure 2. (a) Specular and (b) in-plane X-ray diffraction patterns for a (Ti-Se)2-(Bi-Se)2 precursor after annealing at each temperature for 30 min.

to crystallize $[(BiSe)_{1+\delta}]_2[TiSe_2]_2$. As found in the precursor for $[(BiSe)_{1+\delta}]_1[TiSe_2]_1$, the specular scan of the as-deposited precursor (Figure 2a) contains relatively sharp and intense maxima at small Q resulting from the periodic modulation of the electron density produced by the precursor deposition. At larger Q values, broader maxima are present, consistent with the formation of small domains of the targeted $[(BiSe)_{1+\delta}]_2[TiSe_2]_2$ compound. The in-plane diffraction scan of the as-deposited precursor contains broad, low-intensity reflections that are consistent with small amounts of crystalline BiSe and TiSe₂. As the annealing temperature is increased, reflections at larger Q values grow in intensity in the specular scan. The reflections

from the initial elemental modulation shift as the annealing temperature increases, such that by 250 °C all of the specular reflections approach that expected from a single family of 00l reflections. The superlattice is aligned to the substrate with a caxis lattice parameter of 23.792(2) Å determined from the large Q reflections. The intensity of the reflections for BiSe and TiSe₂ in the in-plane diffraction scans also increases as the annealing temperature is increased. The growth of BiSe and TiSe2 as well as the observed superlattice reflections is consistent with the formation of the targeted $[(BiSe)_{1+\delta}]_2[TiSe_2]_2$ compound. Annealing at 250 °C results in the largest intensities of the reflections attributed to $[(BiSe)_{1+\delta}]_2[TiSe_2]_2$ in both the specular and in-plane diffraction scans. These are the first data that suggest that BiSe layers thicker than one bilayer can be formed in heterostructures.

Annealing at 300 and 350 °C results in changes to the diffraction patterns that indicate that $[(BiSe)_{1+\delta}]_2[TiSe_2]_2$ transforms into $[(BiSe)_{1+\delta}]_1[TiSe_2]_1$. At 300 °C, the intensity of odd order 00l reflections in the specular diffraction pattern decays, while the even 00l reflections become more intense. Despite these changes, the in-plane pattern contains only hk0 reflections from BiSe and TiSe₂, suggesting that the m = 2superstructure is decomposing into $[(BiSe)_{1+\delta}]_1[TiSe_2]_1$. By 350 °C, the 00*l* reflections solely from $[(BiSe)_{1+\delta}]_2[TiSe_2]_2$ are nearly absent and the remaining reflections can be indexed to the $[(BiSe)_{1+\delta}]_1[TiSe_2]_1$ superstructure. $[(BiSe)_{1+\delta}]_2[TiSe_2]_2$ is only kinetically stable as it decomposes at elevated annealing temperatures into $[(BiSe)_{1+\delta}]_1[TiSe_2]_1$.

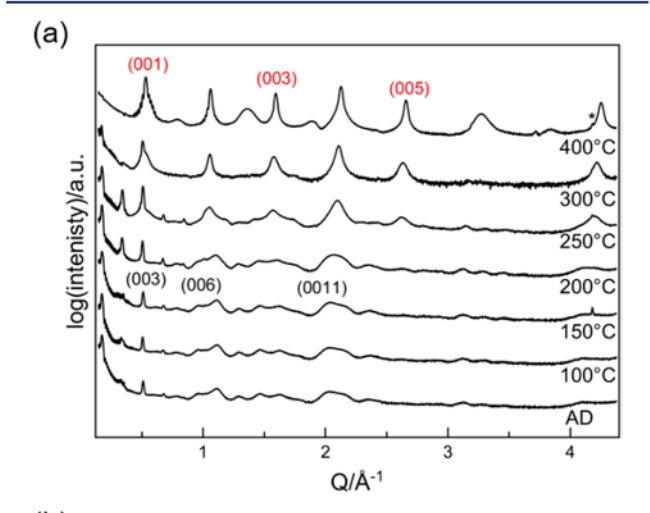
Table 2 summarizes the changes in the lattice parameters corresponding to the targeted $[(BiSe)_{1+\delta}]_2[TiSe_2]_2$ compound

Table 2. Lattice Parameters for (Ti-Se)₂-(Bi-Se)₂ Precursor after Annealing at Each Temperature for 30 min

annealing temp (°C)	c (Å)	BiSe a (Å)	BiSe b (Å)	TiSe ₂ a (Å)
AD	24.08(1)	4.55(3)	4.23(2)	3.56(1)
100	24.06(1)	4.51(1)	4.22(1)	3.59(1)
200	23.991(2)	4.597(6)	4.222(4)	3.591(3)
250	23.792(2)	4.581(6)	4.230(5)	3.587(1)
300	23.725(1)	4.562(4)	4.233(3)	3.577(1)
350	23.689(1)	4.558(2)	4.240(2)	3.579(1)
400		4.558(1)	4.250(1)	3.604(5)

after each annealing temperature. The c-axis lattice parameter decreases as annealing temperature increases, reflecting increased order as the atoms arrange to form [(Bi-Se)_{1+ δ}]₂[TiSe₂]₂. Annealing at temperatures greater than 200 °C causes the difference between the BiSe a and b in-plane lattice parameters to decrease; however there is an insignificant change in the in-plane area. Annealing at 300 °C and above results in the in-plane lattice parameters of both constituents converging toward the lattice parameters of [(Bi-Se)_{1+ δ}]₁[TiSe₂]₁. This is consistent with the evolution of the specular diffraction pattern and supports the hypothesis that the targeted $[(BiSe)_{1+\delta}]_2[TiSe_2]_2$ compound decomposes into $[(BiSe)_{1+\delta}]_1[TiSe_2]_1$ (indices shown in red in Figure 2a). At 400 °C, reflections in both the specular and in-plane diffraction patterns indicate that Bi₂Se₃ is present. This is consistent with the data presented on the annealing of $[(BiSe)_{1+\delta}]_1[TiSe_2]_1$, which clearly shows that at these elevated temperatures [(BiSe)_{1+δ}]₁[TiSe₂]₁ reacts with oxygen and releases Se²⁻ ions, which react with the BiSe layers to form Bi2Se3. The small difference in the TiSe₂ lattice parameters of [(BiSe)_{1+ δ}]₁[TiSe₂]₁ formed through decomposition (a = 3.604(5)) and $[(BiSe)_{1+\delta}]_1[TiSe_2]_1$ formed from a designed precursor (a = 3.580(3)) may reflect differences in composition due to defects and/or the concentration of antiphase boundaries in the BiSe layer.

Specular (Figure 3a) and in-plane (Figure 3b) diffraction scans were also collected after annealing the (Ti-Se)3-(Bi-



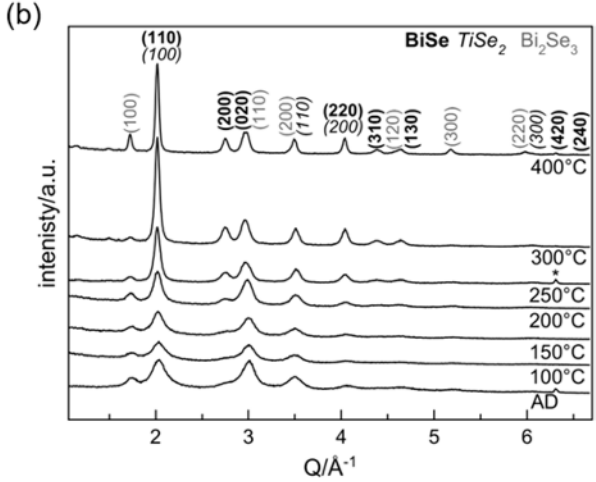


Figure 3. (a) Specular and (b) in-plane X-ray diffraction patterns for a (Ti-Se)₃-(Bi-Se)₃ precursor after annealing at each temperature for 30 min.

Se)₃ precursor at various temperatures. Like the previously discussed precursors, the as-deposited specular diffraction scan contains small Q diffraction maxima from the designed compositional modulation and broad Bragg reflections at larger Q indicating some long-range order due to self-assembly during deposition. The as-deposited in-plane diffraction scan contains reflections expected for BiSe and TiSe2 and weak reflections that are consistent with the presence of a small amount of Bi_2Se_3 . Below 200 °C, there are only slight increases in both inplane lattice parameters of BiSe and a decrease in the a-axis lattice parameter of TiSe2 (Table 3), suggesting that there is little interdiffusion and/or self-assembly occurring.

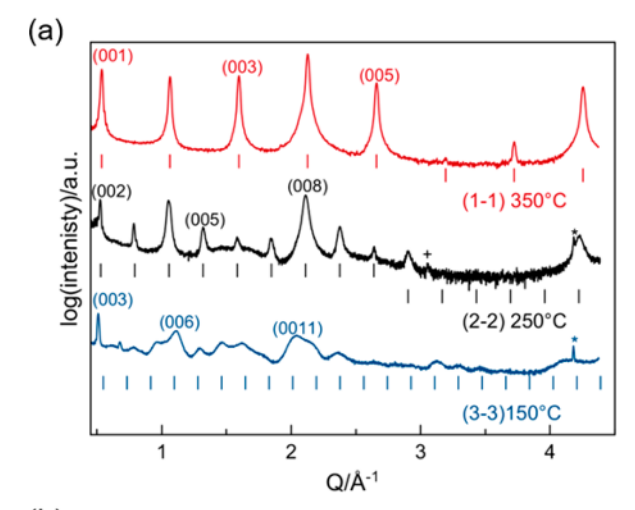
At 200 °C and above, there are significant changes to the structure of the (Ti-Se)₃-(Bi-Se)₃ precursor. In the 200 °C specular scans, a series of reflections appear at low Q values, consistent with a repeat spacing of 37.2(2) Å. The reflection at

Table 3. Lattice parameters for (Ti-Se)₃-(Bi-Se)₃ Precursor after Annealing at Each Temperature for 30 min

annealing temp (°C)	BiSe a (Å)	BiSe b (Å)	TiSe ₂ a (Å)
AD	4.50(1)	4.23(1)	3.616(2)
100	4.46(2)	4.23(1)	3.592(3)
150	4.54(1)	4.25(1)	3.583(2)
200	4.557(3)	4.258(3)	3.576(1)
250	4.547(2)	4.242(2)	3.567(1)
300	4.553(1)	4.240(1)	3.575(1)
400	4.564(1)	4.255(1)	3.597(1)

approximately $2.1~\mbox{Å}^{-1}$ changes from two overlapped reflections at lower temperatures to a broad reflection at 200 °C. The reflections at higher Q values are not consistent with the reflections at low Q values, yielding a repeat spacing of 34.3(2) Å. At 250 °C the reflections in the specular diffraction scan expected for $[(BiSe)_{1+\delta}]_1[TiSe_2]_1$ grow in intensity, an additional reflection grows in at low Q, and the higher Q reflections do not change in intensity. At 300 °C the specular diffraction pattern is consistent with that expected for $[(BiSe)_{1+\delta}]_1[TiSe_2]_1$. The in-plane diffraction patterns show only growth of hk0 reflections for BiSe and TiSe2 when annealed at a temperature of 300 °C and below. The evolution of the (Ti-Se)₃-(Bi-Se)₃ precursor at lower temperatures is more complex than observed for the (Ti-Se)₂-(Bi-Se)₂ precursor, but it also evolves into $[(BiSe)_{1+\delta}]_1[TiSe_2]_1$ after annealing at 300 °C. At 400 °C, reflections for Bi₂Se₃ appear in the specular scan and the Bi₂Se₃ reflections in the in-plane scan become much more intense. This is consistent with the oxidation of $[(BiSe)_{1+\delta}]_1[TiSe_2]_1$ discussed previously.

Figure 4 shows a comparison of the specular and in-plane diffraction patterns of the (Ti-Se)₁I(Bi-Se)₁, (Ti-Se)₂I(Bi-Se)2, and (Ti-Se)3 (Bi-Se)3 precursors annealed at their optimum temperatures to form their targeted compound. The diffraction pattern of the annealed (Ti-Se), I(Bi-Se), precursor contains sharp, defined reflections in both specular and in-plane geometries, indicating that the compound $[(BiSe)_{1+\delta}]_1[TiSe_2]_1$ has formed with a high degree of crystallinity. The c-axis lattice parameter obtained from the diffraction pattern, 11.81(2) Å, is slightly larger than that reported previously (11.77 Å).²² The specular diffraction pattern of the annealed (Ti-Se)2|(Bi-Se)2 precursor is consistent with the formation of the targeted [(Bi-Se)_{1+ δ}]₂[TiSe₂]₂ compound; however the low-Q reflections are shifted to slightly lower angles than expected from the positions of the higher Q reflections. This reflects contributions to the intensity from the artificial layering of the precursor, resulting in a c-axis of 24.06(3) Å calculated from the first three reflections.31 The remaining, higher Q, reflections yield a c-axis of 23.79(2) Å, as they are dominated by intensity from the crystalline compound. The c-axis lattice parameter of the crystalline compound is about 0.2 Å greater than twice the caxis lattice parameter of $[(BiSe)_{1+\delta}]_1[TiSe_2]_1$. This difference results from the different interfaces present in the two materials and implies that the BiSe-BiSe bilayer spacings or the TiSe₂-TiSe₂ van der Waals gap is larger than the BiSe-TiSe₂ van der Waals gap. 32,33 This may suggest that greater attractive forces exist between BiSe-TiSe2 interfaces compared to the BiSe-BiSe or TiSe₂-TiSe₂ interfaces, which provides a rationale as to why the compounds become increasingly unstable as the relative number of BiSe-TiSe2 interfaces decreases. The specular diffraction pattern of the annealed (Ti-Se)31(BiJournal of the American Chemical Society



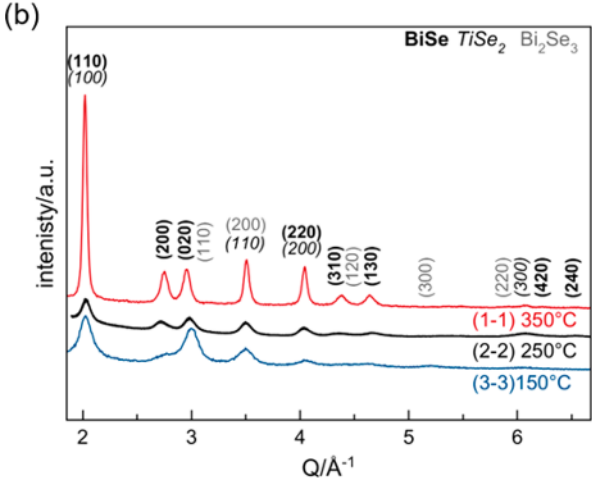


Figure 4. (a) Specular and (b) in-plane X-ray diffraction patterns for $[(BiSe)_{1+\delta}]_2[TiSe_2]_2$ and $[(BiSe)_{1+\delta}]_3[TiSe_2]_3$ compounds prior to evidence of decomposition are compared to the $[(BiSe)_{1+\delta}]_1[TiSe_2]_1$ compound after annealing each to the listed temperature for 30 min. Tick marks are added to (a) as a visual aid of the location of the reflections from the calculated lattice parameters.

Se)₃ precursor contains reflections from two sources. The sharp, defined reflections at small Q values that grow in intensity during annealing yield a repeating thickness of 37.2(2) Å. The broader reflections at larger Q values can be indexed as a single family of reflections, yielding a c-axis lattice parameter of 34.3(2) Å. Since the difference between the lattice parameters of $[(BiSe)_{1+\delta}]_2[TiSe_2]_2$ and $[(BiSe)_{1+\delta}]_1[TiSe_2]_1$ is 12 Å, an estimate for the expected lattice parameter of $[(BiSe)_{1+\delta}]_3[TiSe_2]_3$ is \sim 36.3 Å, which is between these two values. This suggests that, at best, there is only partial self-assembly of the targeted $[(BiSe)_{1+\delta}]_3[TiSe_2]_3$ compound.

The reflections present in the in-plane diffraction scan of the annealed samples support this interpretation of the specular diffraction patterns. The reflections in the in-plane diffraction pattern of $[(BiSe)_{1+\delta}]_1[TiSe_2]_1$ are sharper than those present in $[(BiSe)_{1+\delta}]_2[TiSe_2]_2$, and all reflections in patterns collected at 300 °C or less can be indexed as either BiSe or $TiSe_2$ reflections. The BiSe reflections in the in-plane diffraction pattern of the annealed $(Ti-Se)_3|(Bi-Se)_3$ precursor are less defined and broader than those in the other compounds. These data suggest that the $[(BiSe)_{1+\delta}]_2[TiSe_2]_2$ compound is less crystalline than $[(BiSe)_{1+\delta}]_1[TiSe_2]_1$, and the $[(BiSe)_{1+\delta}]_3[TiSe_2]_3$ compound is even less well crystallized,

highlighting the difficulty of synthesizing these kinetically stable compounds.

The stability difference between the three compounds can be understood through a simple parallel plate capacitor model. Assuming complete charge donation of one electron per BiSe bilayer to the TiSe2, one could calculate the stabilization energy due to the ionic attraction between the layers using the following equation: $V_m = 1/(4\pi\varepsilon_m)(-m^2e^2/r_m)$, where ε_m is the permittivity of the material between the layers, e is the elementary charge, me is the charge of the layers, and r_m is the distance between the charges. For m = 1, we assume that r_1 is the distance between the BiSe and TiSe₂ layers and ε_1 is the permittivity of the van der Waals gap. If charge is concentrated at the surface of the layers r_m remains the distance between the BiSe and TiSe2 layers. As m is increased, one would expect greater stability for $[(BiSe)_{1+\delta}]_m[TiSe_2]_m$ relative to m $[(BiSe)_{1+\delta}]_1[TiSe_2]_1$ layers because the stabilization energy increases as m^2 . However, because BiSe is a semiconductor and TiSe₂ is a small band gap semiconductor or a semimetal (dependent on defect concentration), a space charge region will form at the interface on the two materials. The separation of the charges will be larger than the distance between the BiSe-TiSe₂ van der Waals gap. If the c-axis lattice parameter is smaller than the charge depletion width, then the separation between the charges scales with the c-axis lattice parameter. Since the c-axis lattice parameter is proportional to m, r_m is proportional to mr1. As the depletion width grows, the dielectric constant separating the charges is that of the van der Waals gap plus a portion of the layers themselves. This results in a larger value for the permittivity, $\varepsilon_m > \varepsilon_1$, and leads to less stabilization for $[(BiSe)_{1+\delta}]_m[TiSe_2]_m$ relative to m $[(BiSe)_{1+\delta}]_1[TiSe_2]_1$ layers.

Cross-sectional HAADF-STEM images of the (Ti-Se)2|(Bi-Se)₂ precursor annealed at pre- and postdecomposition temperatures were collected to gain information about the local structure and the structural rearrangements that occur with decomposition. Figure 5 shows a representative HAADF-STEM image of the $[(BiSe)_{1+\delta}]_2[TiSe_2]_2$ precursor annealed at 250 °C, the temperature where the compound is best formed. The image indicates that the average structure comprises two BiSe bilayers alternating with two TiSe₂ layers; however, the sample contains many defects. Numerous substitutional defects are present, where part of a BiSe layer is replaced by a TiSe₂ layer and vice versa. The average period estimated from this image is consistent with the c-axis lattice parameter of the superlattice, calculated from the specular diffraction. Where visible, the zone axis orientations differ in each layer, which is consistent with the turbostratic disorder observed previously in (BiSe)_{1,15}TiSe₂ prepared via the same self-assembly approach. 22,34 Where a TiSe₂ (110) zone axis is visible, it is clear that TiSe2 is a 1T polytype. The different zone axis orientations of the BiSe layer are consistent with a distorted rock salt structure. When the BiSe layer is orientated along a (110) zone axis, so-called antiphase boundaries can be found, where two Bi atoms are adjacent to one another.³⁵ The limited spatial extent of the zone axis domains indicates the layers comprise many small grains, which is consistent with the broad reflections observed in the in-plane diffraction.

Figure 6 contains a representative HAADF-STEM of the $(Ti-Se)_2|(Bi-Se)_2$ precursor annealed at 400 °C. The image contains two distinct regions, one containing [(Bi-Se)_{1+ δ}]₁[TiSe₂]₁ and the other Bi₂Se₃ resulting from the reaction of [(BiSe)_{1+ δ}]₁[TiSe₂]₁ with oxygen. During the

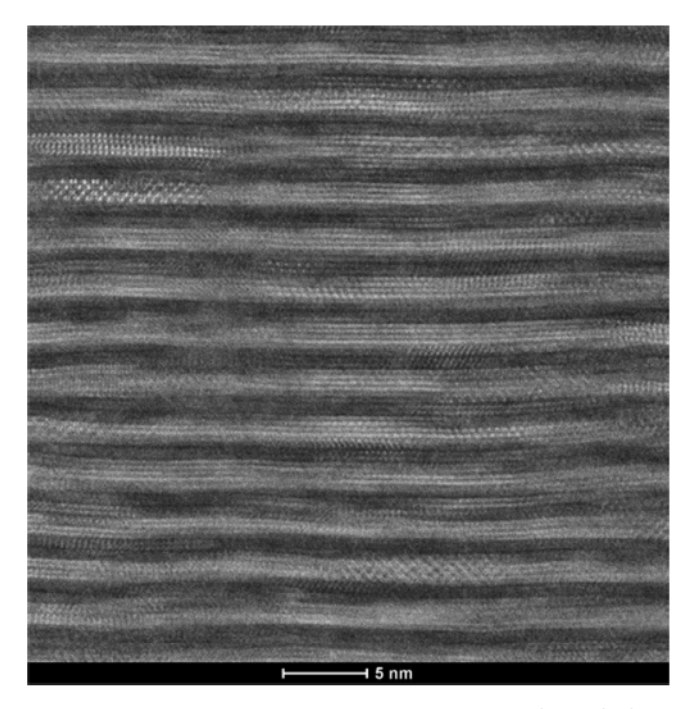


Figure 5. Cross-sectional HAADF-STEM image of the (Ti-Se)2|(Bi-Se)₂ precursor annealed to 250 °C. The gray scale contrast differentiates the different atomic species, with the Bi-containing regions appearing bright compared to the darker regions that contain Ti atoms.

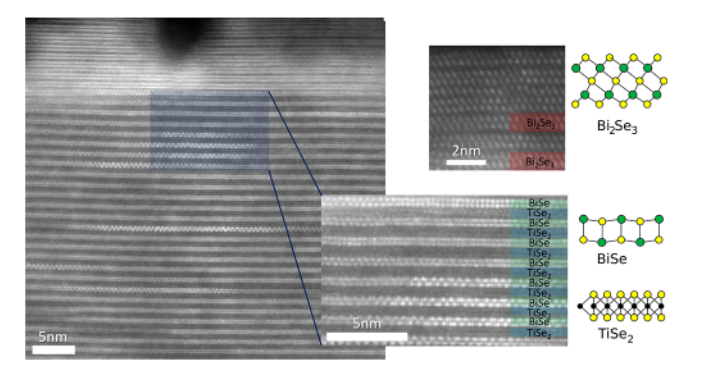


Figure 6. Cross-sectional HAADF-STEM image of the (Ti-Se)2|(Bi-Se)₂ precursor annealed to 400 °C. The sample is predominately $[(BiSe)_{1+\delta}]_1[TiSe_2]_1$ (inset, bottom), capped by textured Bi_2Se_3 (inset, top).

rearrangement of $[(BiSe)_{1+\delta}]_2[TiSe_2]_2$ to $[(BiSe)_{1+\delta}]_1[TiSe_2]_{1}$ atoms must diffuse perpendicular to the layering. The Bi₂Se₃ phase is segregated to the surface of the film as reaction with oxygen is likely a gas-solid reaction. The Bi₂Se₃ has a preferred alignment with respect to the substrate, in agreement with the diffraction data. The $[(BiSe)_{1+\delta}]_1[TiSe_2]_1$ is under the Bi_2Se_3 , and the interfaces between the BiSe and TiSe2 layers are atomically smooth. The $[(BiSe)_{1+\delta}]_1[TiSe_2]_1$ region is remarkably defect free considering the low annealing temperature and short annealing times required to transform from [(Bi- $[Se)_{1+\delta}]_2[TiSe_2]_2$. Antiphase boundaries are present in the BiSe layer, as reported previously. The visible zone axis changes orientations layer to layer, consistent with turbostratic disorder. The Bi₂Se₃ region contains more defects, including regions where it appears that BiSe monolayers separate Bi₂Se₃ layers. These defects likely result from the nonstoichiometry

resulting from the disproportionation of the (Ti-Se)2 (Bi-Se)2 precursor.

DSC data were collected on the three (Ti-Se),, |(Bi-Se),, precursors to further probe the formation and subsequent decomposition with increased annealing temperature (Figure 7). The DSC scan of the (Ti-Se)₁|(Bi-Se)₁ precursor contains

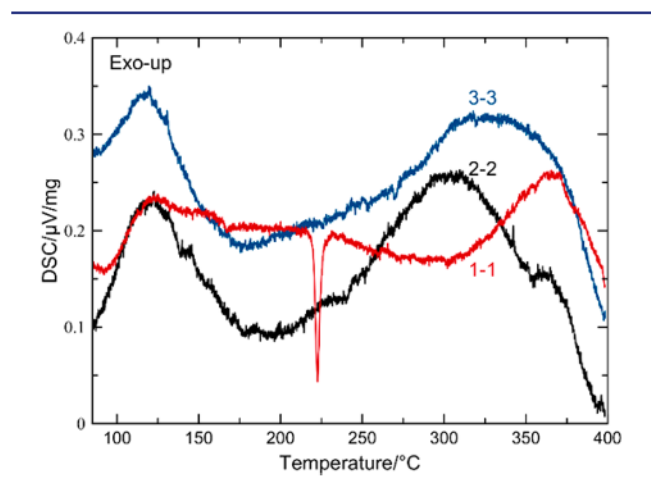


Figure 7. Differential scanning calorimetry data for the 1-1 (red), 2-2 (black), and 3-3 (blue) as-deposited precursor.

a broad exotherm that starts at approximately 125 °C, an endotherm at approximately 220 °C, and a second broad exotherm with a maximum heat flow at approximately 375 °C. The sharp endotherm at 220 °C is from the melting of Se in the precursor. The exotherm at 375 °C is the oxidation of the sample. The DSC scan of the (Ti-Se)₂-(Bi-Se)₂ precursor contains two broad exotherms, with one maximum heat flow at approximately 125 °C and the second at approximately 300 °C. The diffraction data collected as a function of annealing suggest that the low-temperature exotherm results from the formation of the $[(BiSe)_{1+\delta}]_2[TiSe_2]_2$. The HAADF-STEM and diffraction data suggest that the higher temperature exotherm results from the transformation of $[(BiSe)_{1+\delta}]_2[TiSe_2]_2$ into [(Bi- $Se)_{1+\delta}$ ₁[TiSe₂]₁. The high-temperature shoulder on this exotherm is the oxidation of $[(BiSe)_{1+\delta}]_1[TiSe_2]_1$ and correlates with the appearance of Bi₂Se₃ in the X-ray diffraction annealing study. The scan of the (Ti-Se)3-(Bi-Se)3 precursor contains a low-temperature exotherm with a maximum heat flow at approximately 125 °C and a second higher temperature exotherm with a maximum heat flow at approximately 350 °C. The diffraction data suggest that the smaller lowtemperature exotherm results from partial self-assembly of the targeted $[(BiSe)_{1+\delta}]_3[TiSe_2]_3$ compound and that the higher temperature exotherm results from the transformation into $[(BiSe)_{1+\delta}]_1[TiSe_2]_1.$

The results presented here suggest that BiSe-TiSe2containing heterostructures exist in local free energy minima as depicted in Figure 8 with a qualitative schematic of the structures. The compounds become increasingly less stable as m, the thickness of the constituent layers, is increased. This corresponds to the decreasing depth of the free energy minima as m increases in Figure 8. When given sufficient energy to overcome the activation barrier associated with solid-state diffusion, the compounds lower their energy by rearranging into $[(BiSe)_{1+\delta}]_1[TiSe_2]_1$, which is the global minimum within this restricted energy landscape. The formation of Bi₂Se₃ as a secondary phase in the annealing experiments suggests that

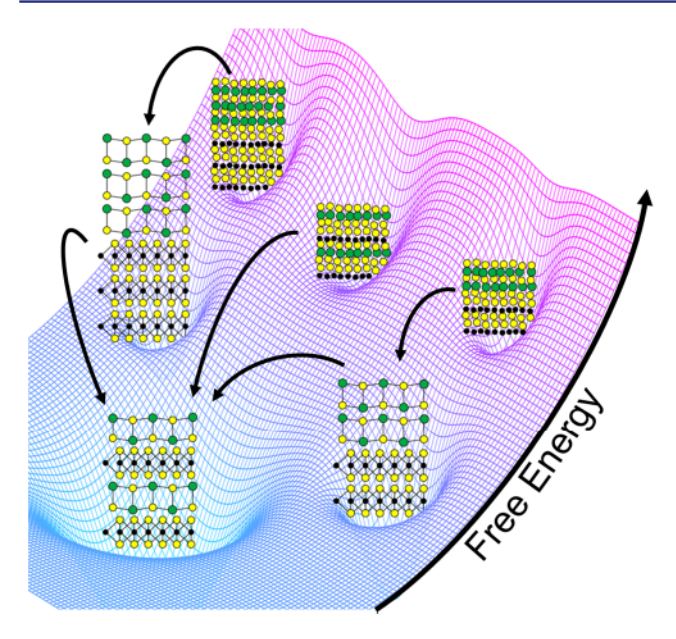


Figure 8. Schematic free energy landscape. The 2-2 and 3-3 compounds exist in shallower local minima than the 1-1 compound and can lower their free energy by rearranging into the 1-1 structure. Arrows indicate transitions from higher energy states (shallower wells) to lower energy states (deeper wells). The schematic images of the asdeposited layers do not depict the small percentage of the films that have already begun to self-assemble into the ordered layers.

intergrowths containing Bi₂Se₃ with TiSe₂ and/or BiSe may be possible under the correct synthesis conditions from appropriately designed precursors.

CONCLUSION

Here we report the synthesis of kinetically stable BiSe-TiSe2containing heterostructures, $[(BiSe)_{1+\delta}]_m[TiSe_2]_m$ for $m \leq 3$. Specular X-ray diffraction, collected after annealing at various temperatures, revealed the formation and subsequent decomposing of the targeted superlattices. The m = 2 and 3 compounds decomposed into $[(BiSe)_{1+\delta}]_1[TiSe_2]_1$. At higher temperatures $[(BiSe)_{1+\delta}]_1[TiSe_2]_1$ reacts with traces of oxygen, forming Bi₂Se₃ on the surface. The compounds become increasingly unstable as m is increased. These results demonstrate that kinetically stable compounds exist in a complex free energy landscape defined by the interactions within and between the constituents. While many members of a homologous series of compounds can be imagined, the complex free energy landscape governs which compounds can be formed and highlights the difficulty of synthesizing multiple members of a potential homologous series of compounds, especially those with identical stoichiometry. The results of this Article demonstrate that chemists can gain valuable qualitative knowledge of the free energy landscape through studies of precursors designed to produce different members of a homologous series.

AUTHOR INFORMATION

Corresponding Author

*davej@uoregon.edu

ORCID ®

Alexander C. Lygo: 0000-0003-1762-244X Danielle M. Hamann: 0000-0002-9262-1060 Marco Esters: 0000-0002-8793-2200

Suzannah R. Wood: 0000-0002-7208-7681 David C. Johnson: 0000-0002-1118-0997

Notes

The authors declare no competing financial interest.

ACKNOWLEDGMENTS

Author A.C.L. acknowledges support from the University of Oregon Office of the Vice President of Research and Innovation (VPRI) and the Presidential Undergraduate Research Scholarship (PURS). This Article is based upon work supported by the National Science Foundation Graduate Research Fellowship Program under Grant No. 1309047. The authors acknowledge support from the National Science Foundation under Grant DMR-1710214. We would like to acknowledge the Center for Advanced Materials Characterization in Oregon (CAMCOR) at the University of Oregon. We acknowledge support through the Collaborative Access Team (CAT): Pooled Resources for Electron Microscopy Informatics, Education and Research (PREMIER) Network Program at Pacific Northwest National Laboratory (PNNL) and the Environmental Molecular Sciences Laboratory, a national scientific user facility sponsored by the DOE's Office of Biological and Environmental Research at PNNL. PNNL is a multiprogram national laboratory operated by Battelle for the DOE under Contract DE-AC05-76RL01830. The Los Alamos National Laboratory is operated by Los Alamos National Security, LCC, for the National Nuclear Security Administration of the U.S. Department of Energy under Contract No. DE-AC52-06NA2539. The authors thank Evguenia A. Karapetrova at 33-BM-C for technical assistance during collection of the synchrotron XRD data. This research used resources of the Advanced Photon Source, a U.S. Department of Energy (DOE) Office of Science User Facility operated for the DOE Office of Science by Argonne National Laboratory under Contract No. DE-AC02-06CH11357

REFERENCES

- (1) Wang, X. L.; Sakurai, H.; Takayarria-Muromachi, E. J. Appl. Phys. 2005, 97, 10M519.
- (2) Tian, W.; Haeni, J. H.; Schlom, D. G.; Hutchinson, E.; Sheu, B. L.; Rosario, M. M.; Schiffer, P.; Liu, Y.; Zurbuchen, M. A.; Pan, X. Q. Appl. Phys. Lett. 2007, 90, 22507.
- (3) Maeno, Y.; Hashimoto, H.; Yoshida, K.; Nishizaki, S.; Fujita, T.; Bednorz, J. G.; Lichtenberg, F. Nature 1994, 372, 532-534.
- (4) Moritomo, Y.; Asamitsu, A.; Kuwahara, H.; Tokura, Y. Nature 1996, 380, 141-144.
- (5) Kanatzidis, M. G. S. Acc. Chem. Res. 2005, 38, 359-368.
- (6) Kabbour, H.; Cario, L. Inorg. Chem. 2006, 45, 2713-2717.
- (7) Cario, L.; Kabbour, H.; Meerschaut, A. Chem. Mater. 2005, 17, 234-236.
- (8) Schön, J. C.; Jansen, M. Angew. Chem., Int. Ed. Engl. 1996, 35, 1286 - 1304
- (9) Jansen, M.; Schön, J. C. Angew. Chem., Int. Ed. 2006, 45, 3406-
- (10) Ohno, Y. Phys. Rev. B: Condens. Matter Mater. Phys. 1991, 44, 1281-1291.
- (11) Ettema, A. R. H. F.; Haas, C. J. Phys.: Condens. Matter 1993, 5, 3817-3826.
- (12) Ettema, A. R. H. F.; Haas, C.; Turner, T. S. Phys. Rev. B: Condens. Matter Mater. Phys. 1993, 47, 12794-12805.
- (13) Fang, C. M.; Van Smaalen, S.; Wiegers, G. A.; Haas, C.; de Groot, R. A. J. Phys.: Condens. Matter 1996, 8, 5367-5382.
- (14) Brandt, J.; Kipp, L.; Skibowski, M.; Krasovskii, E. E.; Schattke, W.; Spiecker, E.; Dieker, C.; Jäger, W. Surf. Sci. 2003, 532-535, 705-710.

- (15) Kalläne, M.; Rossnagel, K.; Marczynski-Bühlow, M.; Kipp, L.; Starnberg, H. I.; Stoltz, S. E. Phys. Rev. Lett. 2008, 100, 065502.
- (16) Beauvais, L. G.; Shores, M. P.; Long, J. R. Chem. Mater. 1998, 10, 3783-3786.
- (17) Noh, M.; Thiel, J.; Johnson, D. C. Science 1995, 270, 1181-1184.
- (18) Hamann, D. M.; Hadland, E.; Johnson, D. C. Semicond. Sci. Technol. 2017, 32, 93004.
- (19) Trump, B. A.; Livi, K. J. T.; McQueen, T. M. J. Solid State Chem. 2014, 209, 6-12.
- (20) Oosawa, Y.; Gotoh, Y.; Akimoto, J. J. Alloys Compd. 1991, 176, 319-327.
- (21) Gotoh, Y.; Onoda, M.; Uchida, K.; Tanaka, Y.; Iida, T.; Hayakawa, H.; Oosawa, Y. Chem. Lett. 1989, 18, 1559-1562.
- (22) Merrill, D. R.; Moore, D. B.; Coffey, M. N.; Jansons, A. W.; Falmbigl, M.; Johnson, D. C. Semicond. Sci. Technol. 2014, 29, 64004.
- (23) Atkins, R.; Wilson, J.; Zschack, P.; Grosse, C.; Neumann, W.; Johnson, D. C. Chem. Mater. 2012, 24, 4594-4599.
- (24) Phung, T. M.; Jensen, J. M.; Johnson, D. C.; Donovan, J. J.; McBurnett, B. G. X-Ray Spectrom. 2008, 37, 608-614.
- (25) Akselrud, L.; Grin, Y. J. Appl. Crystallogr. 2014, 47, 803-805.
- (26) Le Bail, A.; Duroy, H.; Fourquet, J. L. Mater. Res. Bull. 1988, 23, 447–452.
- (27) Roisnel, T.; Rodríquez-Carvajal, J. Mater. Sci. Forum 2001, 378–381, 118–123.
- (28) Rodríguez-Carvajal, J. Phys. B 1993, 192, 55-69.
- (29) Kang, H.-J.; Kim, J.; Oh, J.; Back, T.; Kim, H. Microsc. Microanal. 2010, 16, 170-171.
- (30) Schaffer, M.; Schaffer, B.; Ramasse, Q. Ultramicroscopy 2012, 114, 62-71.
- (31) Fullerton, E. E.; Schuller, I. K.; Vanderstraeten, H.; Bruynseraede, Y. Phys. Rev. B: Condens. Matter Mater. Phys. 1992, 45, 9292-9310.
- (32) Anderson, M. D.; Heideman, C. L.; Lin, Q.; Smeller, M.; Kokenyesi, R.; Herzing, A. A.; Anderson, I. M.; Keszler, D. A.; Zschack, P.; Johnson, D. C. Angew. Chem., Int. Ed. 2013, 52, 1982–1985.
- (33) Beekman, M.; Disch, S.; Rouvimov, S.; Kasinathan, D.; Koepernik, K.; Rosner, H.; Zschack, P.; Neumann, W. S.; Johnson, D. C. Angew. Chem., Int. Ed. 2013, 52, 13211–13214.
- (34) Wood, S. R.; Merrill, D. R.; Falmbigl, M.; Moore, D. B.; Ditto, J.; Esters, M.; Johnson, D. C. Chem. Mater. 2015, 27, 6067–6076.
- (35) Hyde, B. G.; Bagshaw, A. N.; Andersson, S.; O'Keeffe, M. Annu. Rev. Mater. Sci. 1974, 4, 43-92.
- (36) Mitchson, G.; Falmbigl, M.; Ditto, J.; Johnson, D. C. Inorg. Chem. 2015, 54, 10309-10315.
- (37) Mitchson, G.; Hadland, E.; Göhler, F.; Wanke, M.; Esters, M.; Ditto, J.; Bigwood, E.; Ta, K.; Hennig, R. G.; Seyller, T.; et al. ACS Nano 2016, 10, 9489–9499.